Active Vibration Control of a Cantilever Beam using Electromagnetic Actuators

Kangwoong Ko, Sooyoung Choi and Kiheon Park

Abstract - In this paper, an experiment for the active vibration control of a cantilever beam uses electromagnet as an actuator and uses a laser sensor to measure the position of the bending beam, constituting a non-contacting control system. A mathematical model of the overall system is derived to analytically design an appropriate controller. Dynamic equations of the electromagnetic actuator and the beam are combined to find the transfer function from the actuator to the sensor. The effectiveness of the obtained model is verified by various experiments and an improper PID controller is designed based on the obtained model. According to analysis, the coefficient of the derivative controller is the most important parameter for handling the performance and the stability margin of the control system. The experimental results of the active control system are compared with those of the open loop system.

Keywords - active vibration control, electromagnets, PID controls, noncollocated system

1. Introduction

Active vibration control of flexible structures has been the interest of many researchers[1,2,5,7]. Most research and development efforts treat integrated structures with actuators, sensors, and control systems. Different electroactive materials, such as piezoelectric ceramics, shape memory alloys, and electromagnets, are being considered as actuators and/or sensors of active vibration control systems. Piezoelectric ceramics have been the most popular materials due to their high stiffness, good linearity, and low temperature sensitivity[1,2]. These materials are, however, attached to the flexible structures to improve damping of the structures, which limits them to applications where non-contacting control methods are needed. An electromagnet is a useful device for non-contacting control sehemes and is used as an actuator in such applications as electromagnetic suspension, magnetic bearings, and electromagnet dampers. Okada et al.[7] and Matsuda et al.[5] treat active vibration control of steel sheets using magnetic actuators. Though they deal with a non-contacting vibration control problem, their main concern lies in the design of effective electro-magnetic actuators. The vibrational dynamics of the steel sheet is not analyzed and an improper PID controller is presented with no analysis. In fact, the controller design procedures and characteristics of the controller are not mentioned. In this paper, a non-contacting vibration control problem is treated for a cantilever beam, and, notably, a mathemat ical model of the overall system is presented. Dynamic equations of the electromagnetic actuator and the beam are combined to find the transfer function from the electromagnetic actuator to the laser sensor. The force formula of the electromagnets is adopted from Matsuda[5] and the transfer characteristics of the beam is derived via the model analysis[6] of vibrating beams. Effectiveness of the obtained model is verified by comparing experimental and simulated results. Fine tuning the parameters of the model minimizes the discrepancy between them. Based on the obtained model, a PID controller is designed via various simulation trials, and experiments verify that this PID controller works as well as predicted in the simulati on. Analyzing the obtained model in this paper indicates that the derivative term of the PID controller is the most important for handling the tradeoff between performance and stability margin.

This work was supported by the Korea Science and Engineering Foundation under grant R01-2000-000-00252-0.

Manuscript received: Feb. 14, 2002 accepted: June 14, 2002

Kangwoong Ko is with the Mechatronics Center, SamSung Electronics Co. Ltd, Suwon, Korea.

Sooyoung Choi and Kiheon Park are with School of Information and Communications Engineering at SungKyunKwan University, Suwon. Korea.

2. A vibration control system and its modeling

The experimental setup for an active vibration control system is depicted in Fig.1. The control objective of this experiment is to increase the damping ratio of the cantilever beam by controlling the input current to the magnetic actuator in response to the laser sensor output. A cantilever is a projecting beam supported at only one end and is frequently used as a test structure to examine vibration phenomena.

The feedback control system model of the experimental system is given in Fig.2 where the plant $P(s)$ denotes the

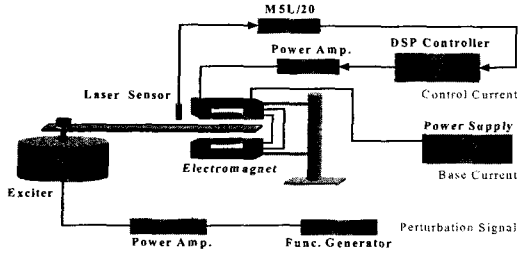

Fig. 1 An active vibration control system

transfer function from the actuator input(input voltage of the electromagnet) to laser sensor output voltage.

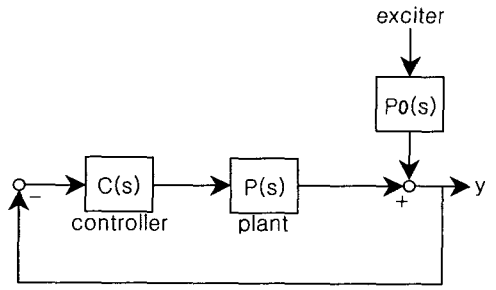

Fig. 2 The modeling of the system in Fig.1

In the remaining part of this section, derivation of the transfer function $P(s)$ is explained. First, we derive the transfer function $P_v(s)$ from force input $f(t)$ at a point on the beam to the displacement $y(t)$ at another point on the beam. Secondly, the transfer function $P_m(s)$ from the voltage input of the magnetic actuator to the magnetic force acting on the beam is derived so that the final transfer function $P(s)$ is obtained as $P_v(s)P_m(s)$.

2.1 Transfer function $P_v(s)$ of the beam

Consider the cantilever beam in Fig.3 where $f(x,t)$ and $y(x,t)$ denote the transverse force per unit length and the bending displacement, respectively.

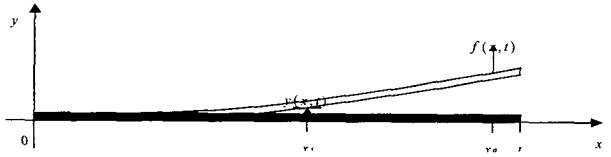

Fig. 3 The clamped-free beam

It is well known[6] that the flexural vibration of the beam is modeled by the differential equation

$$-EI\frac{\partial^4 y(x,t)}{\partial x^4}+f(x,t)=m\frac{\partial^2 y(x,t)}{\partial t^2} \quad (0<x<L). \tag{1}$$

According to modal analysis, we let the solution of this equation have the form

$$y(x,t)=\sum_{r=1}^{\infty} Y_r(x)\cdot q_r(t) \tag{2}$$

where $Y_r(x)$ is the r-th mode function of the beam and $q_r(t)$ is the time function to be determined. The mode functions are given explicitly as

$$\begin{aligned} Y_r(x)=&\frac{C_{1r}}{(\sin\beta_r L-\sinh\beta_r L)}\\ &\{(\sin\beta_r L-\sinh\beta_r L)(\sin\beta_r x-\sinh\beta_r x)\\ &+(\cos\beta_r L+\cosh\beta_r L)(\cos\beta_r x-\cosh\beta_r x)\} \end{aligned} \tag{3}$$

$$C_{1r}=\frac{1}{\sqrt{m}}\sigma_r,\quad \sigma_r=\frac{(\sinh\beta_r L-\sin\beta_r L)}{(\cosh\beta_r L+\cos\beta_r L)} \tag{4}$$

$$\beta_1 L=1.87510407,\quad \beta_2 L=4.69409113,\cdots \tag{5}$$

where L and m are the length and the mass per unit length of the beam, respectively. The mode function $Y_r(x)$ satisfies the ortho-normal properties

$$\int_0^L mY_r(x)\,Y_s(x)\,dx=\delta_{rs}=\begin{Bmatrix}0 & r\neq s\\ 1 & r=s\end{Bmatrix} \tag{6}$$

$$\int_0^L Y_s(x)EIY_r^{(4)}(x)\,dx=\omega_r^2\delta_{rs},\quad \omega_r=\beta_r^2\sqrt{\frac{EI}{m}} \tag{7}$$

where EI is the flexural rigidity of the beam. Substituting Eq.(2) into Eq.(1), we obtain

$$\begin{aligned} m\Big(\sum_{r=1}^{\infty}Y_r(x)\cdot\ddot{q}_r(t)\Big)+EI\Big(\sum_{r=1}^{\infty}Y_r^{(4)}(x)\cdot q_r(t)\Big)\\ =f(x,t)\quad (0<x<L). \end{aligned} \tag{8}$$

Multiplying $Y_n(x)$, $n=1,2,\cdots$, to both sides of Eq.(8) and integrating from 0 to L, we obtain

$$\begin{aligned} &\sum_{r=1}^{\infty}\int_0^L mY_r(x)Y_n(x)\,\ddot{q}_r(t)dx+\\ &EI\sum_{r=1}^{\infty}\int_0^L Y_r^{(4)}(x)Y_n(x)\,q_r(t)dx=\int_0^L Y_n(x)f(x,t)\,dx \end{aligned} \tag{9}$$

and it follows from Eqs.(6) and (7) that

$$\ddot{q}_n(t)+\omega_n^2\cdot q_n(t)=H_n(t),\quad n=1,2,\cdots \tag{10}$$

$$H_n(t)=\int_0^L Y_n(x)\cdot f(x,t)dx. \tag{11}$$

It is reasonable to insert a damping term into Eq.(10) to consider an damping effect existent in real systems[6] and this results in

$$\ddot{q}_n(t)+2\zeta_n\omega_n\cdot\dot{q}_n(t)+\omega_n^2\cdot q_n(t)=H_n(t),\ n=1,2,\cdots. \tag{12}$$

Next, we let

$$f(x,t)=\delta(x-x_a)f_0(t) \tag{13}$$

to derive the transfer function $P_v(s)$. Here, the actuating force is exerted at $x=x_a$ on the beam. Inserting Eq.(13)

into Eq.(11) yields $H_n(t) = Y_n(x_a)f_0(t)$, and hence

$$Q_n(s) = \frac{F_0(s) \cdot Y_n(x_a)}{s^2+2\zeta_n\omega_n s+\omega_n^2} \tag{14}$$

where $Q_n(s)$ and $F_0(s)$ denote the Laplace transforms of $q_n(t)$ and $f_0(t)$, respectively. From Eq.(2), the bending displacement at $x = x_a$ becomes

$$y(x_s, t) = \sum_{n=1}^{\infty} Y_n(x_s)q_n(t) \tag{15}$$

and performing the Laplace transform of Eq.(15) yields

$$Y(x_s, s) = \left(\sum_{n=1}^{\infty} \frac{Y_n(x_s)Y_n(x_a)}{s^2+2\zeta_n\omega_n s+\omega_n^2} \right) \cdot F_0(s). \tag{16}$$

The transfer function $P_v(s)$ is now obtained as

$$\begin{aligned} P_v(s) &= Y(x_s, s)/F_0(s) \\ &= \sum_{n=1}^{\infty} \frac{Y_n(x_s)Y_n(x_a)}{s^2+2\zeta_n\omega_n s+\omega_n^2}, \end{aligned} \tag{17}$$

and only the first and the second modes will be considered in this paper so that

$$P_v(s) = \frac{Y_1(x_a)Y_1(x_s)}{s^2+2\zeta_1\omega_1 s+\omega_1^2} + \frac{Y_2(x_a)Y_2(x_s)}{s^2+2\zeta_2\omega_2 s+\omega_2^2}. \tag{18}$$

2.2 Transfer function $P_m(s)$ of the electromagnet

The push-pull type electromagnet[7] is used in this experiment to avoid the nonlinearity of hysteresis. Two separate coils, the bias coil and the control coil, are wound as shown in Fig.4.

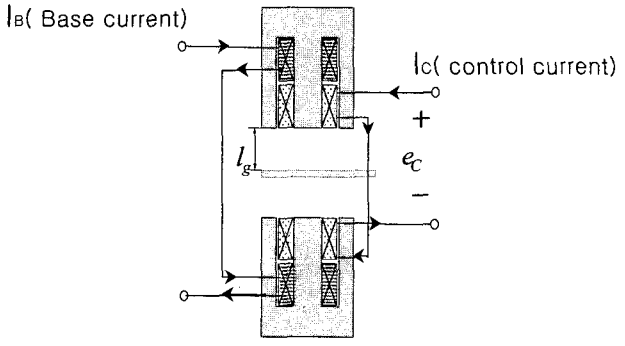

Fig. 4 The push-pull type electromagnet

The connection of the bias coil to both electromagnets is in the same direction. The connection of the control coils is in the opposite direction. We follow Okada's analysis[7] to obtain the input/output relation between the control input current $i_c(t)$ and the electromagnetic force $f_0(t)$ acting on the beam as

$$f_0(t) = \frac{2\mu_0 S_g N_B N_c I_B}{l_g^2} \cdot i_c(t) \tag{19}$$

where μ_0 is permeability of free space, S_g is the cross-sectional area of the electromagnet, N_B is the turns of base coils, N_c is the turns of control coils, I_B is the base current, and l_g is the air gap distance, respectively. Since the electromagnet circuit is modeled by

$$e_c(t) = R_c i_c(t) + L_c \frac{di_c(t)}{dt}, \tag{20}$$

the transfer function $P_m(s) = F_0(s)/E_c(s)$ is given by

$$P_m(s) = k \cdot \frac{2\mu_0 S_g N_B I_B}{l_g^2} \cdot \frac{1}{L_c s + R_c} \tag{21}$$

where k is the constant that adjusts the modeling uncertainties. In fact, there are many factors that make the relation in Eq.(18) inaccurate. For example, the air gap distance l_g is not sufficiently small and the electromagnetic force $f_0(t)$ is distributive in the real system. The role of k is to adjust these uncertainties and its value is to be determined experimentally.

2.3 Tuning of the system transfer function

Combining Eqs.(18) and (21), we obtain the overall transfer function $P(s)$ as

$$P(s) = k \cdot k_L \cdot \frac{2\mu_0 S_g N_B N_c I_B}{l_g^2} \cdot \left(\frac{Y_1(x_a)Y_1(x_s)}{s^2+2\zeta_1\omega_1 s+\omega_1^2} + \frac{Y_2(x_a)Y_2(x_s)}{s^2+2\zeta_2\omega_2 s+\omega_2^2} \right) \cdot \frac{\frac{1}{L_c}}{s+\frac{R_c}{L_c}} \tag{22}$$

where k_L denotes the laser sensor gain. Most parameters in Eq.(22) were determined by measurements of the real experimental system. The important parameters, ω_1, ω_2, ζ_1, ζ_2, and k, were experimentally determined by comparing the signal shapes of the real system with those of the simulated system using the transfer function in Eq.(22). The step and sinusoidal signals were used as test inputs for comparison of transient and steady state responses, respectively. After this fine tuning, we obtained the final transfer function as

$$P(s) = 581.795 \frac{1.4925}{s+334.3} \cdot \left(\frac{1.3072}{s^2+10.178s+41445} + \frac{-1.4451}{s^2+63.27s+1601200} \right) \tag{23}$$

where $\zeta_1 = \zeta_2 = 0.025$, $\omega_1 = 203.58$, and $\omega_2 = 1265.39$.

Fig.5a shows the shape of the actual output signal for a rectangular input, and Fig.5b shows the simulation result using the model in Eq.(23) for the same input in Fig.5a.

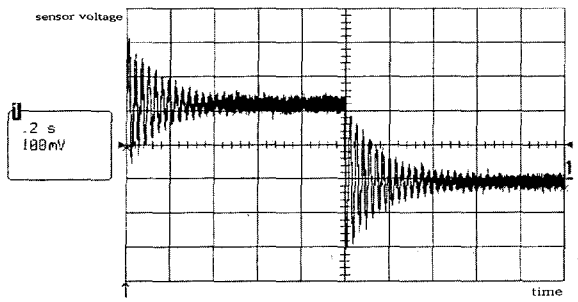

Fig. 5a The output signal of the experiment system for a rectangular input

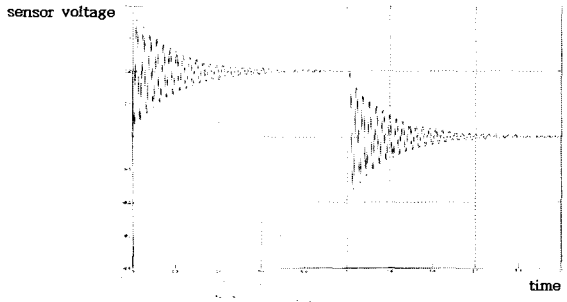

Fig. 5b The simulation result for the same input in Fig.5a

3. Design of the feedback controllers and experimental results

Using the transfer function in Eq.(23), we designed PID controllers to improve damping of the closed loop system. The PID control algorithm was implemented by the DSP controller(TMS320C31) with a sampling time of 1 msec, and bending displacement of the beam was observed by measuring the laser sensor output voltage by a digital oscilloscope. Fig.6 shows the picture of the overall experimental equipment set up.

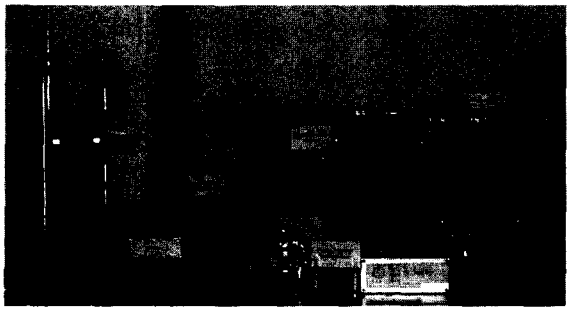

Fig. 6 The experimental setup

3.1 Design of the PID controllers

The transfer function in Eq.(23) has five poles, four of them located near the $j\omega$-axis, and two zeros, one of them located on the positive real axis(refer to Fig.7). This pole-zero configuration is the typical pattern of the non-collocated vibration control system[9]. In fact, due to the physical constraint of the electromagnet and the laser sensor, they cannot be located on the same position and hence our control system is non-collocated, which is known to be harder to control than a collocated system. The following PID controller was considered to improved damping of the closed loop system.

$$C(s) = K(K_P + K_I \cdot \frac{1}{s} + K_D s). \tag{24}$$

In the beginning, proper PI controllers(i.e., $K_D = 0$) were tried to improve damping, but damping improvement PI controllers soon proved unsuccessful(though stabilization of the feedback system was possible). This limitation of the PI controllers is quite understandable when we look into the root locus diagram of the system with a PI controller as in Fig.7a. The locus starting from the first mode pole goes directly to the right side, preventing damping improvement of the feedback system. In contrast, the root locus diagram for a PID controller as shown in Fig.7b enables us to increase damping. Notice that the locus starting from the first mode pole goes to the left side, which indicates improvement of damping. Since the effect of the second mode is small, the location of its locus is unimportant as long as it stays within the left half of the plane. It should be noted that this root locus analysis reveals that any proper controllers, as well as PI controllers, would show poor improvement of damping since the number of poles is not less than that of zeros.

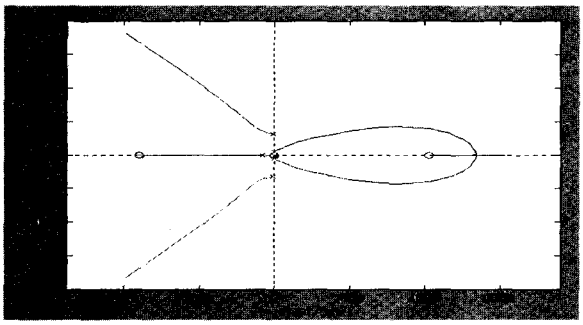

Fig. 7a The root locus diagram with a PI controller

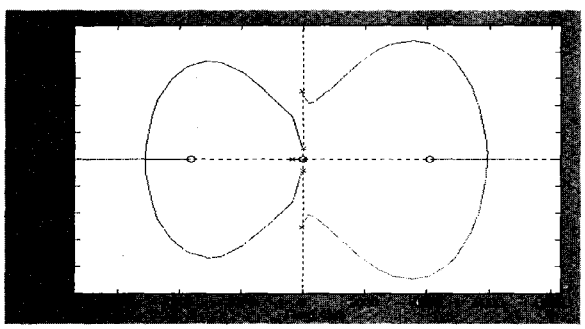

Fig. 7b The root locus diagram with a PID controller

After some trial and error, we find the appropriate PID coefficients and the gain as

$$K=0.1,\ K_P=1,\ K_I=0.1,\ K_D=0.07. \tag{25}$$

Fig. 8 shows the displacement of the beam when a rectangular pulse voltage with a width of 0.01 sec is applied to the electromagnet actuator (the exciter was not activated in this case). Fig.8a is the response for the open loop and Fig.8b is the response for the closed loop with the PID controller.

Fig. 9 denotes the experimental result when the exciter is activated by the sinusoidal signal of the first mode frequency $f_1=32.4Hz$. In the figure, the front part of the response (the larger amplitude part) is the one without the controller and the latter part (the smaller amplitude part) is the response when the PID controller is switched on.

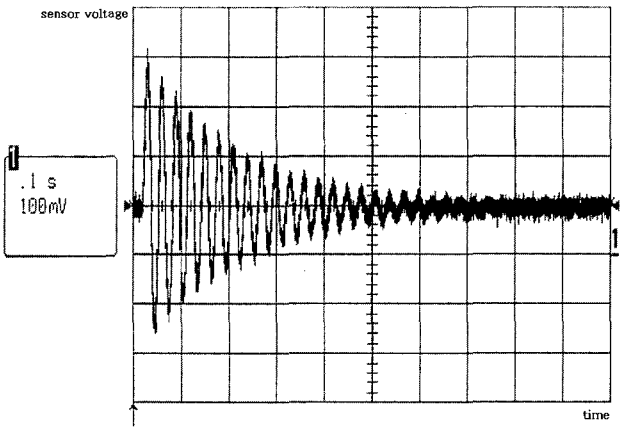

Fig. 8a The response to a rectangular pulse(open loop)

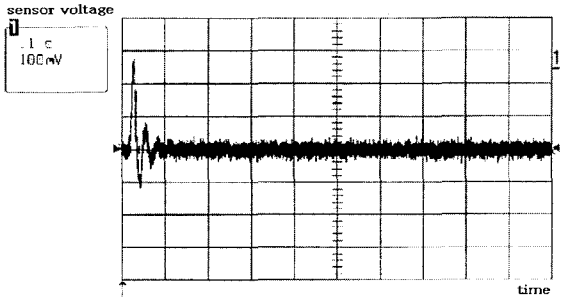

Fig. 8b The response to a rectangular pulse(closed loop)

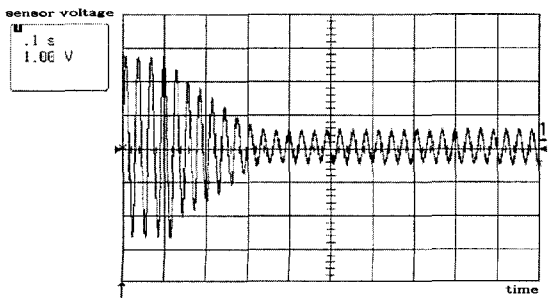

Fig. 9 The response to the sinusoidal exciter input of the first mode frequency(The feedback controller is switched on at t=0.1sec)

3.2 Stability margin analysis

One of the main issues in control system design is the robust analysis. In many applications, the need to satisfy performance specifications is foremost in the design and, hence, the robust stability issue is often omitted. In real situations, however, many uncertainties make optimal performance design based on the nominal model less meaningful and, therefore, robust analysis is a necessary procedure for gaining insight into the operation of the designed system. In this experiment, the parameter K_D turns out to be most important among the three coefficients of the PID controller. Compared to the other coefficients, K_D affects the system response considerably. As K_D increases from 0 to 0.7, the system response, such as the settling time, improves. In general, however, good performance design tend to cause a bad stability margin. Fig.10 shows this case in our experiment. In the figure, the stability margin is defined as the minimal distance between -1 and the Nyquist diagram of the system.

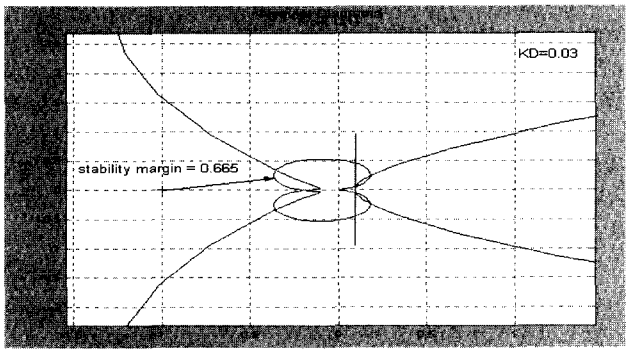

Fig. 10a Stability margin when $K_D=0.03$

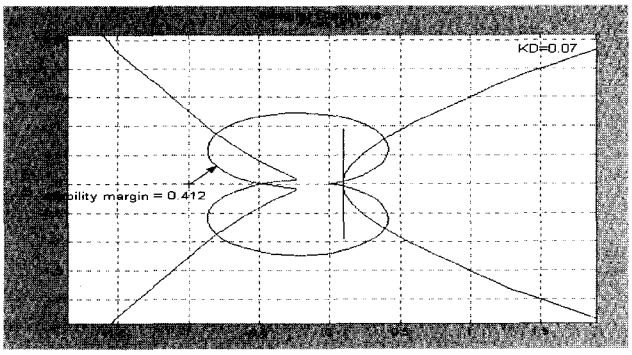

Fig. 10b Stability margin when $K_D=0.07$

As K_D increases, the stability margin decreases, and, hence, when the plant is expected to have severe uncertainties, tradeoff between the performance and the stability margin should be considered seriously.

4. Conclusion and discussions

The experiment of active damping for the cantilever used electromagnets as non-contacting actuators of the control system. The transfer function from the force input to the bending displacement was obtained via modal analysis results. The final transfer function was determined by considering only the first and second modes, and experiments confirmed that this model worked well. PID controllers were shown to improve damping of the beam effectively, and the coefficient K_D was the most important parameter for determining to the perform ance and the stability margin of the control system.

The root locus analysis in Section 3.1 reveals that PI controllers can not improve the damping of the system inherently, and hence adoption of PID controllers is inevitable. It can be, therefore, expected that the controllers adopting the current H_2 or H_∞ algorithm[10] would not improve the damping of the system since the H_2 or H_∞ algorithm always yields proper controllers. In fact, a simple experiment adopting an proper H_2 controller is done and the results show that the previous expectation is right. To overcome this order limitation of the H_2 controllers, research regarding adding a derivative term to the H_2 controllers is in progress.

To satisfy more complex requirements, such as reference tracking and disturbance rejection, we may need to adopt more advanced control algorithms. Especially when the source of vibrational disturbance is known, the feedforward control scheme is known to be very effective in rejecting wide band disturbances[8]. Research regarding combining the feedforward controller with the feedback loop is in progress.

Acknowledgements

This work was supported by the Korea Science and Engineering Foundation under grant R01-2000-000-00252-0.

References

[1] Dosch, J. J., Inman, D. J., and Garcia, E., "A self-sensing piezoelectric actuator for collocated control," Journal of Intelligent Material Systems and Structures, vol. 3, pp.166-185, Jan 1992.

[2] Hagood, N. W., and Von Flotow, A., "Damping of structural vibrations with piezoelectric materials and passive electrical networks," Journal of Sound and Vibrations, vol. 146, no. 2, pp.243-268, 1991.

[3] Kar, I. N., Miyakura, T., and Seto, K., "Bending and torsional vibration control of a flexible plate structure using H_∞-based robust control law," IEEE Transact ions on Control System Technology, vol. 8, no. 3, pp.545-553, May 2000.

[4] Khorrami, F., Zeinoun, I. J., Bongiorno, J. J. Jr., and Nourbakhsh, S., "Application of H_2 design for vibra tion damping and pointing of flexible structures with embedded active materials," Proceedings of American Control Conference, Seattle, WA, pp.4178-4182, June 1995.

[5] Matsuda, K., Yoshihashi, M., Okada, Y., and Tan A.,C., "Self-sensing active suppression of vibration of flexible steel sheet," Journal of Vibration and Accoustics, vol. 118, pp.469-473, July 1996.

[6] Meirovitch L., Elements of Vibration Analysis, McGraw-Hill, 1986.

[7] Okada, Y., Matsumoto, K., and Matsuda, K., "Vibration control of thin steel sheet using flux feedback magnetic actuator," Conference on Motion and Vibration Control, Zurich, Switzerland, vol. 3, pp.1057-1062, August 1998.

[8] Park. K., and Youla, D. C., "Numerical calculation of the optimal three-degree-of-freedom Wiener-Hopf con troller," International Journal of Control, vol. 56, no. 1, pp.227-244, 1992.

[9] Preumont, A., Vibration Control of Active Structures, Kluwer Academic Publishers, 1997.

[10] Doyle, J. C., Glover, K., Khagonekar, P. P. and Francis, B. A., "State-space solutions to standard H_2 and H_∞ control problems," IEEE Transactions on Automatic Control, vol. AC-34, no. 8, pp.831-847, June 1988.

Kangwoong Ko was born in Korea on August 15, 1974. He received his B.S. degree in Electronic Engineering and M.S. degree in the School of Electrical and Computer Engineering from the SungKyunKwan University in 2000 and 2002, respectively. He is currently an engineer with Samsu ng Electronics Co. Ltd. His research interests include vibration control, motion control, and temperature control.

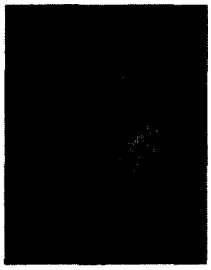

Sooyoung Choi was born in Korea on September 21, 1969. He received his B.S degree in Electrical Engineeri ng and M.S. degree in the School of Electrical and Computer Engineeri ng from the SungKyunKwan Univers ity in 1997 and 1999, respectively. He is currently working toward the Ph.D. degree in the School of Information and Communications Engineering at SungKyunKwan University, Suwon, Korea. His research interests include robust optimal control, man machine interface of an automated machine, and vibration control.

Kiheon Park received the B.S. and M.S. degrees in Electrical Engineeri ng from Seoul National University in 1978 and 1980, respectively, and the Ph.D. degree in Systems Engineering from Polytechnic University, Farmin gdale, NY, in 1987. From 1980 to 1983, he served in the Korean Navy as a full-time instructor at the Naval Academy. During the years 1988-1990, he was involved in a factory automation project at the Electronic and Telecommunications Research Institute, Chungnam, Korea. He is currently a professor of the School of Information and Communications Engineering at SungKyunKwan University, Suwon, Korea. His research interests include Wiener-Hopf design of the linear multivariable control systems, decoupling control systems, vibration control, and industrial control networks. Dr. Park was a recipient of the Korea Electric Association Scholarship from 1983 to 1986.